Supporting Information

Gold(I) Complexes of 2-(diphenylphosphino)aniline: Synthesis and Influence of the Perhalophenyl Ligand on their Assembly

Laura Coconubo-Guio, Sonia Moreno, Miguel Monge, Elena Olmos, José M. López-de-Luzuriaga

[a]*Departamento de Química, Universidad de La Rioja, Centro de Investigación en Síntesis Química (CISQ), Complejo Científico-Tecnológico, 26006 – Logroño, Spain.*

I. Characterization of the complexes

1. IR spectra

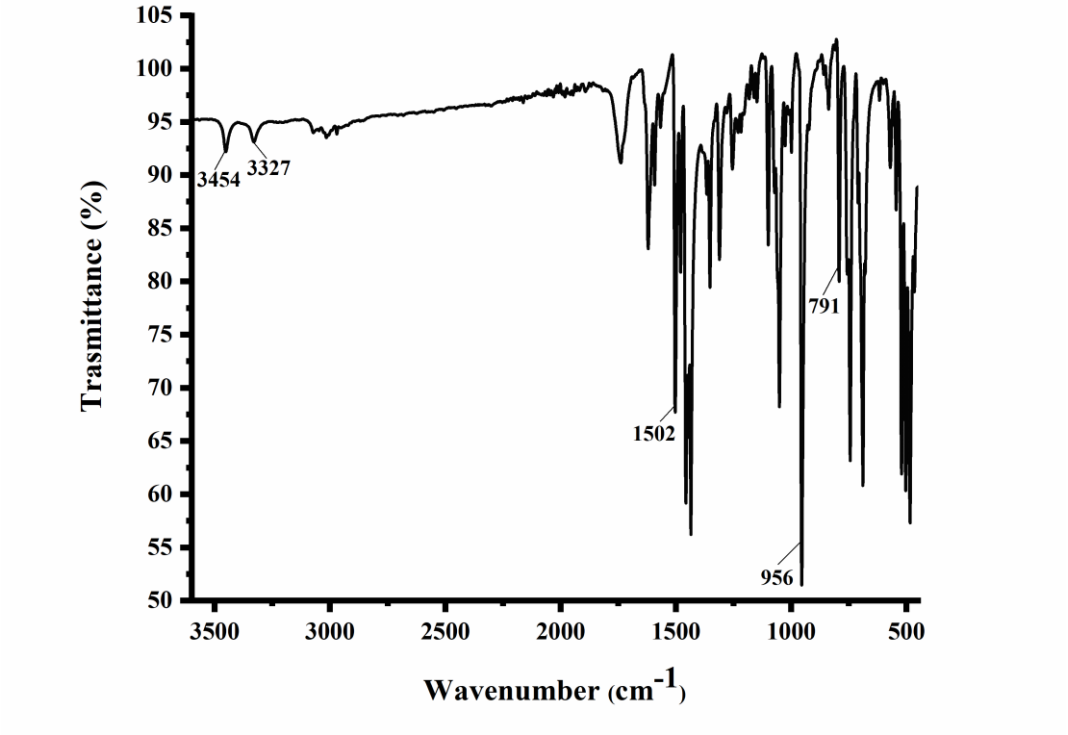

Figure S1. FT-IR spectrum of complex [Au(C_6F_5)(PNH_2)] (**1**)

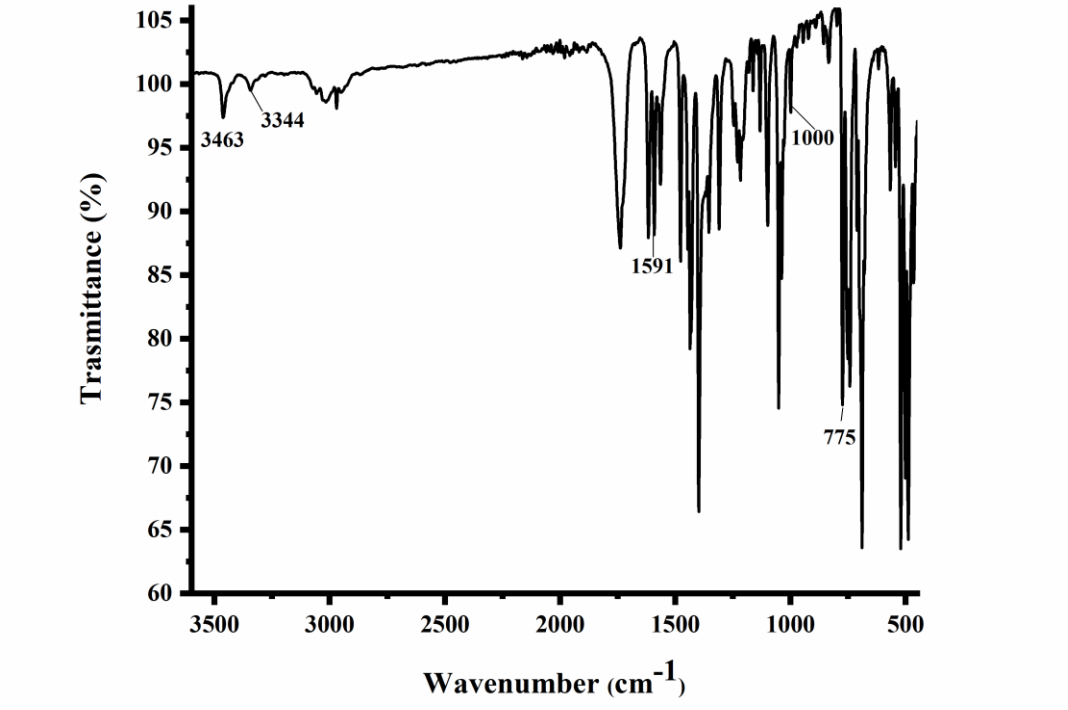

Figure S2. FT-IR spectrum of complex [Au($C_6Cl_2F_3$)(PNH_2)] (**2**)

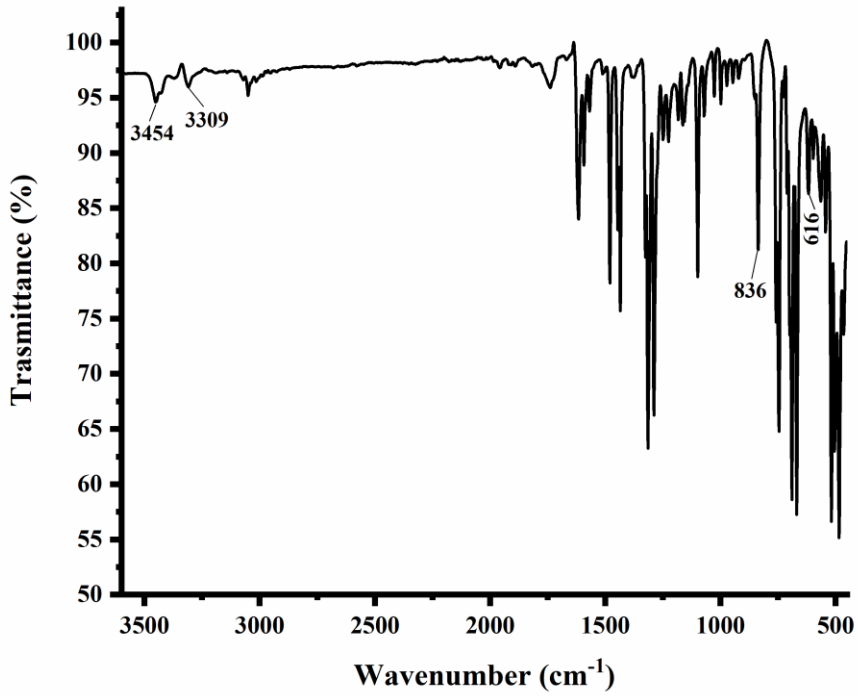

Figure S3. FT-IR spectrum of complex [Au(C_6Cl_5)(PNH_2)] (**3**)

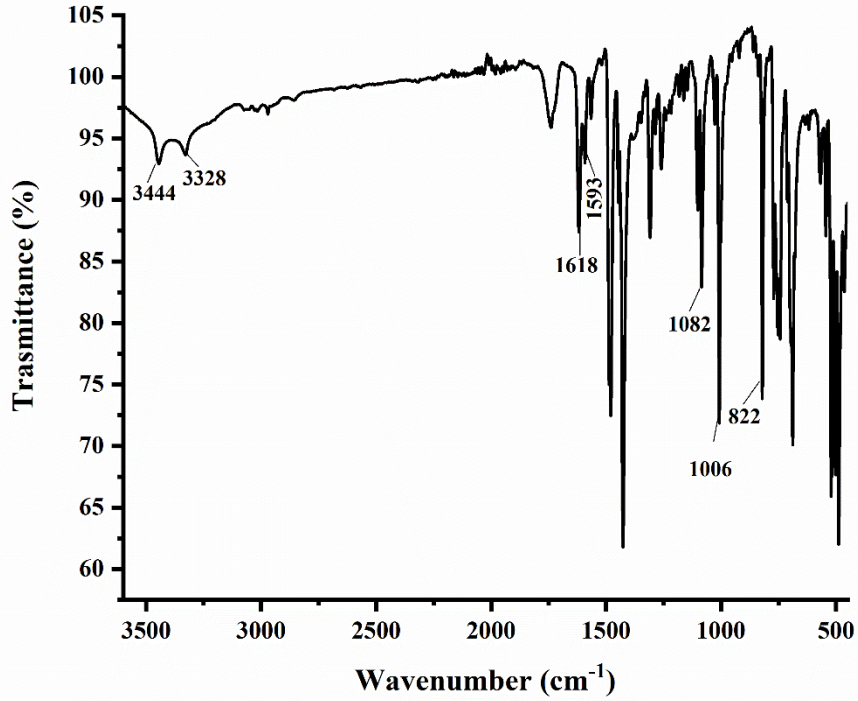

Figure S4. FT-IR spectrum of complex [Au(*o*-C_6BrF_4)(PNH_2)] (**4**)

2. Mass spectrometry data

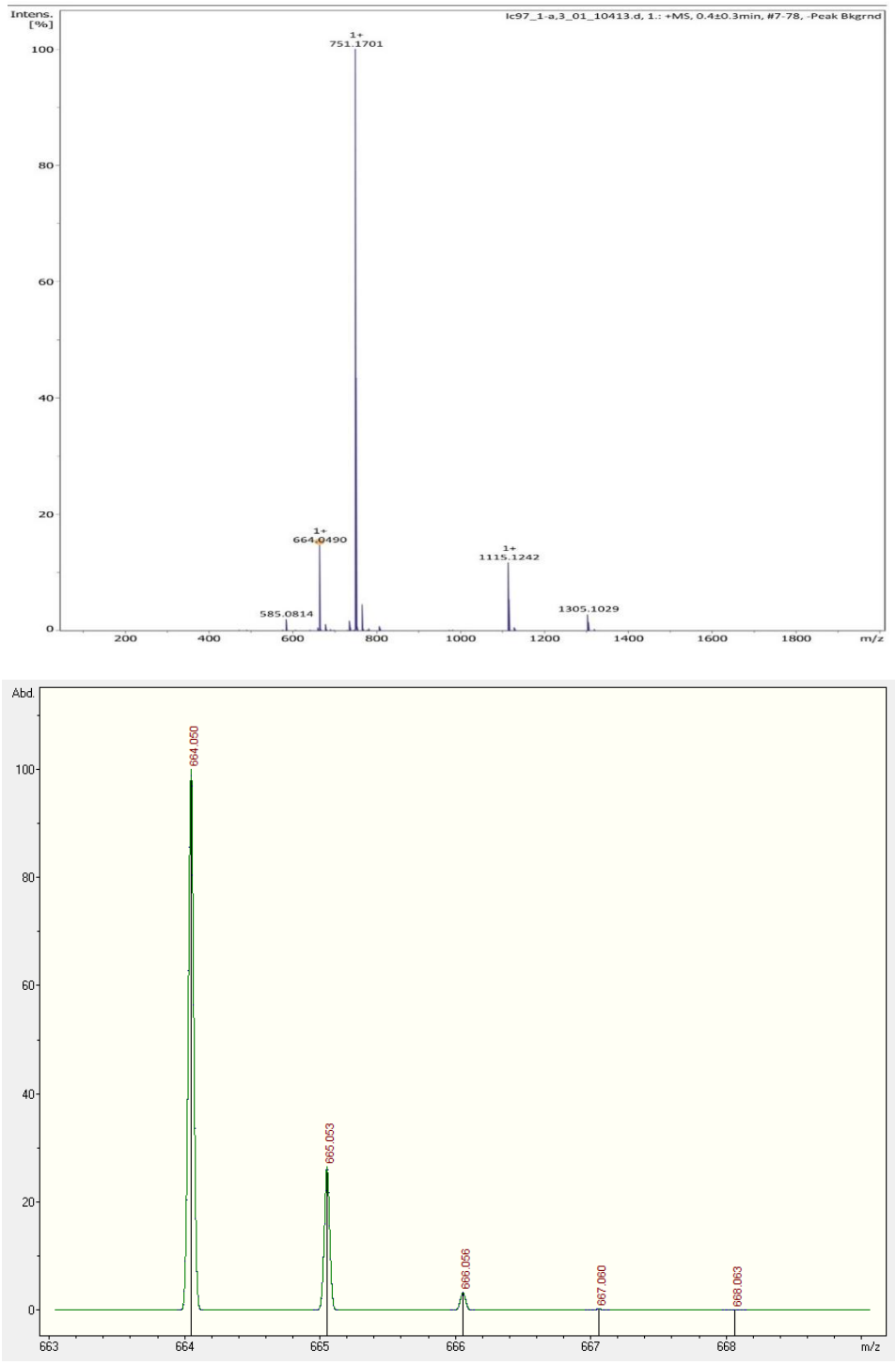

Figure S5. ESI positive of [Au(C_6F_5)(PNH_2)] (1): spectrum of experimental micrOTOF-Q (top) *versus* theoretical (bottom) positive mass spectrometry data

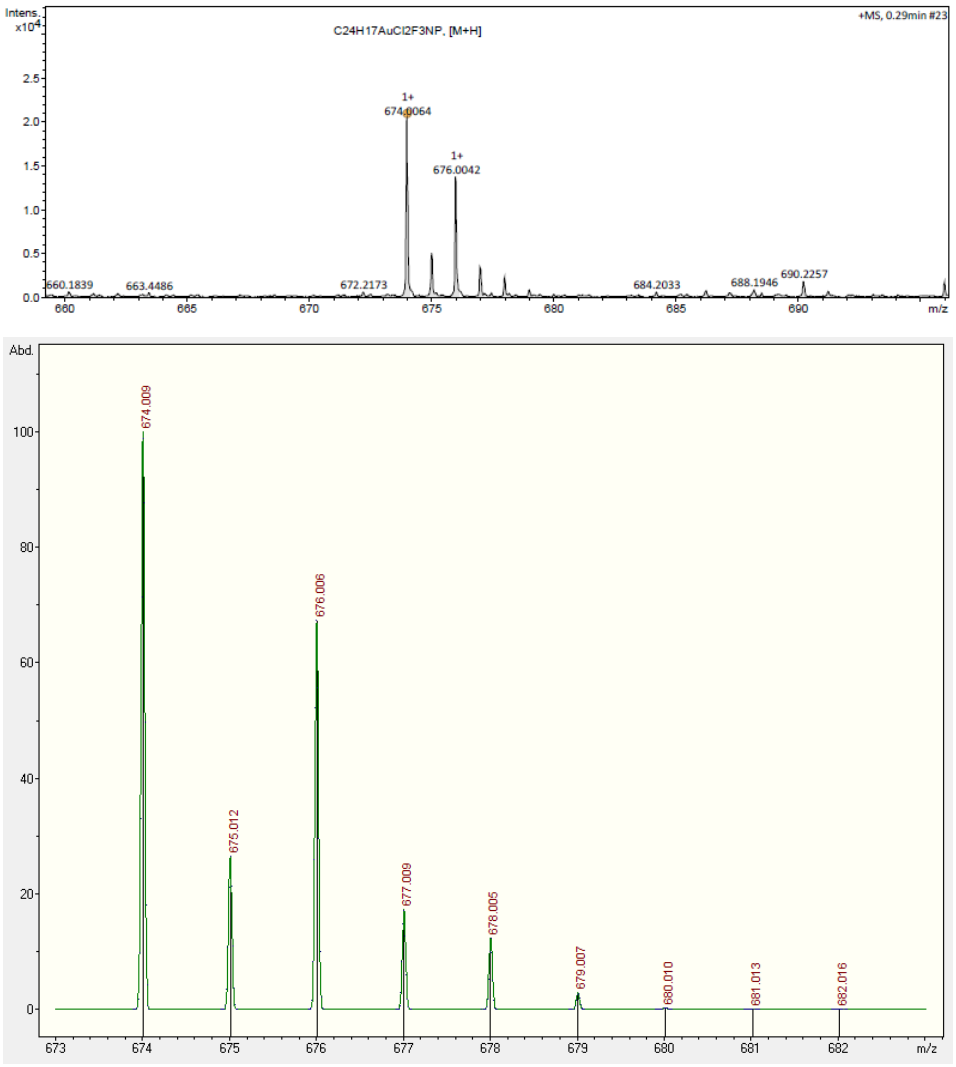

Figure S6. ESI Positive of [Au($C_6Cl_2F_3$)(PNH_2)] (2): spectrum of experimental micrOTOF-Q (top) *versus* theoretical (bottom) positive mass spectrometry data

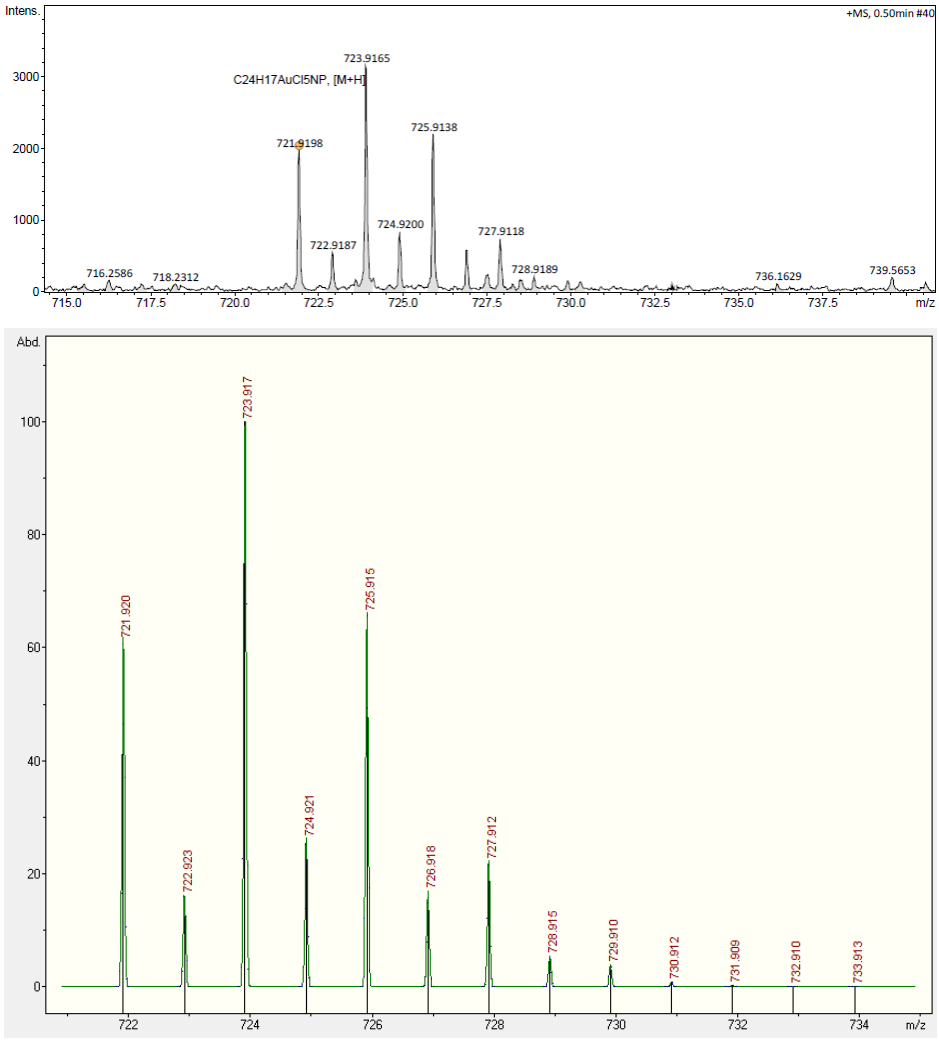

Figure S7. ESI Positive of [Au(C_6Cl_5)(PNH_2)] (3): spectrum of experimental micrOTOF-Q (top) *versus* theoretical (bottom) positive mass spectrometry data

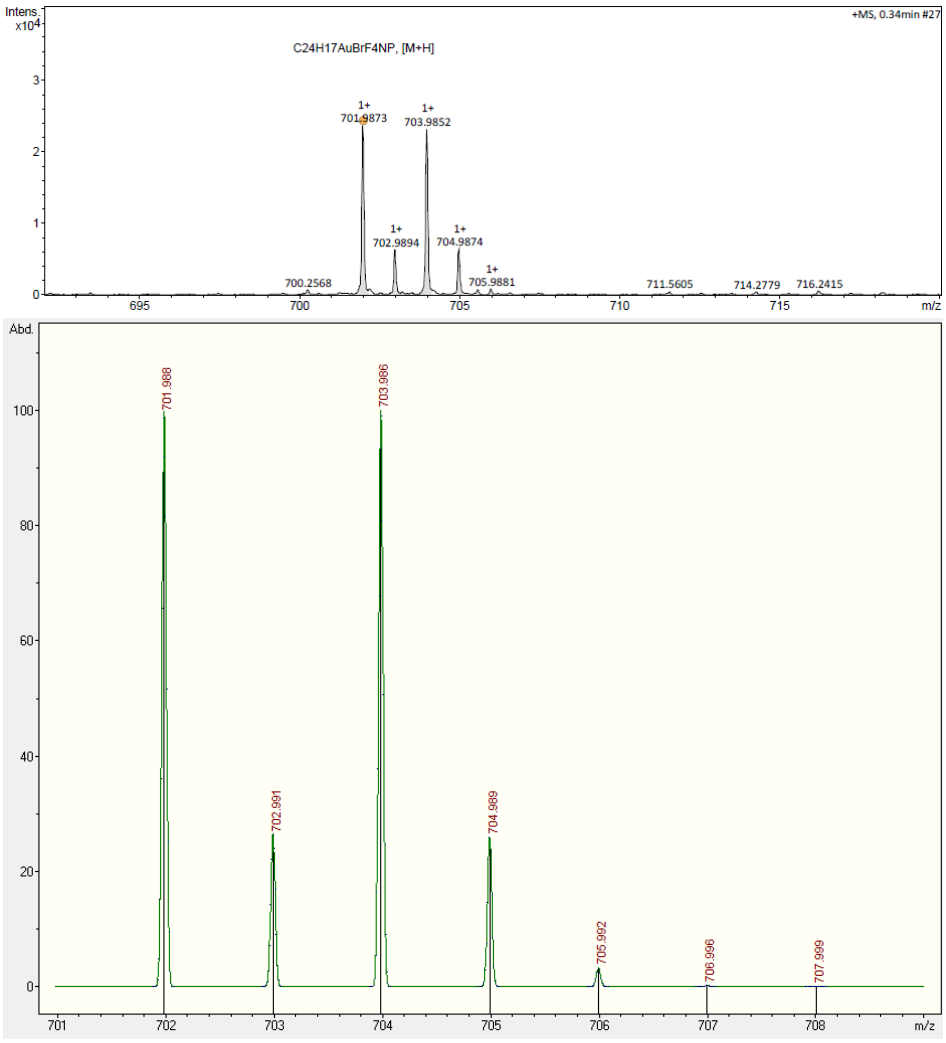

Figure S8. ESI Positive of [Au(*o*-C_6BrF_4)(PNH_2)] (4): spectrum of experimental micrOTOF-Q (top) *versus* theoretical (bottom) positive mass spectrometry data

3. ^{1}H NMR spectra (300 MHz, 298K)

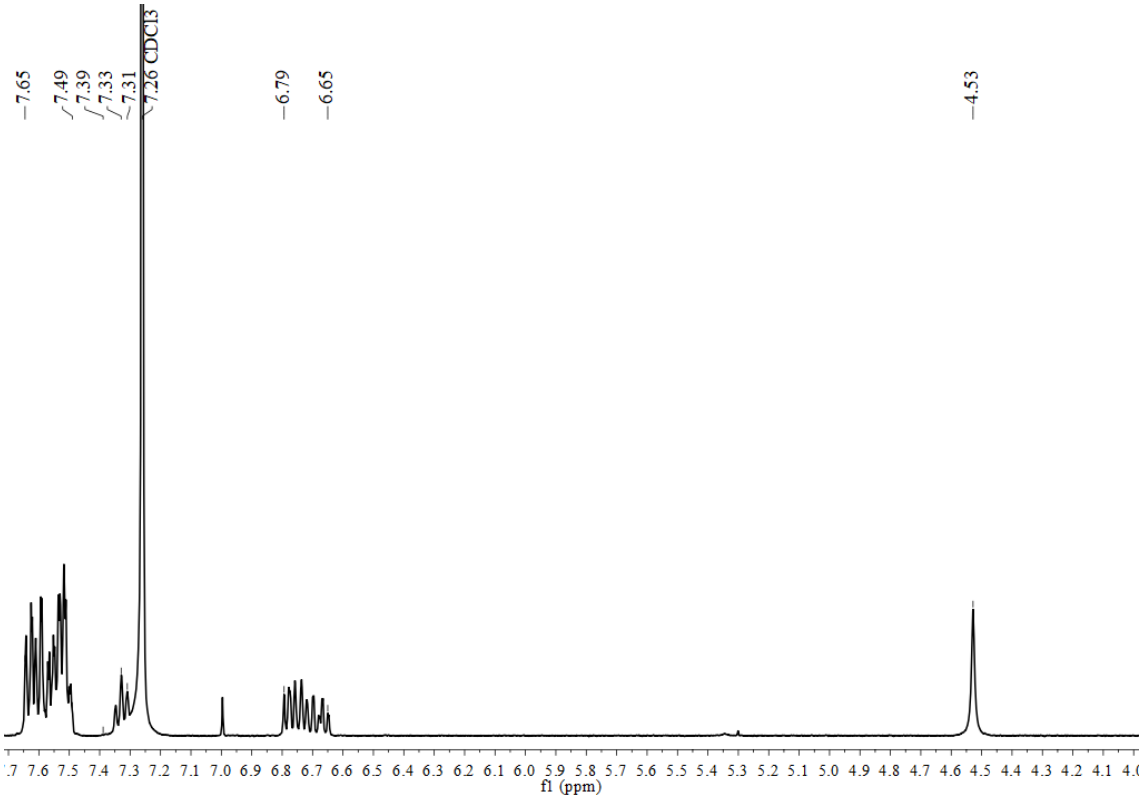

Figure S9. ^{1}H NMR spectrum of complex [Au(C_6F_5)(PNH_2)] (**1**) in $CDCl_3$ 400

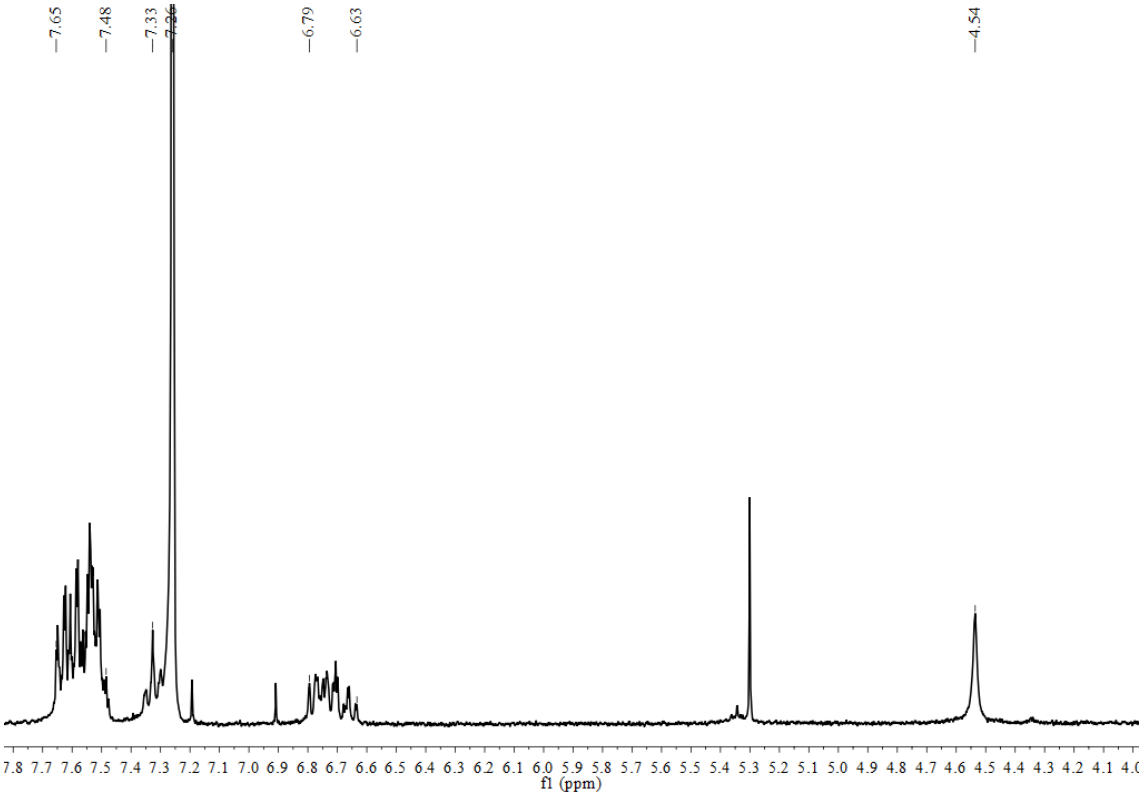

Figure S10. ^{1}H NMR spectrum of complex [Au($C_6Cl_2F_3$)(PNH_2)] (**2**) in $CDCl_3$ 400

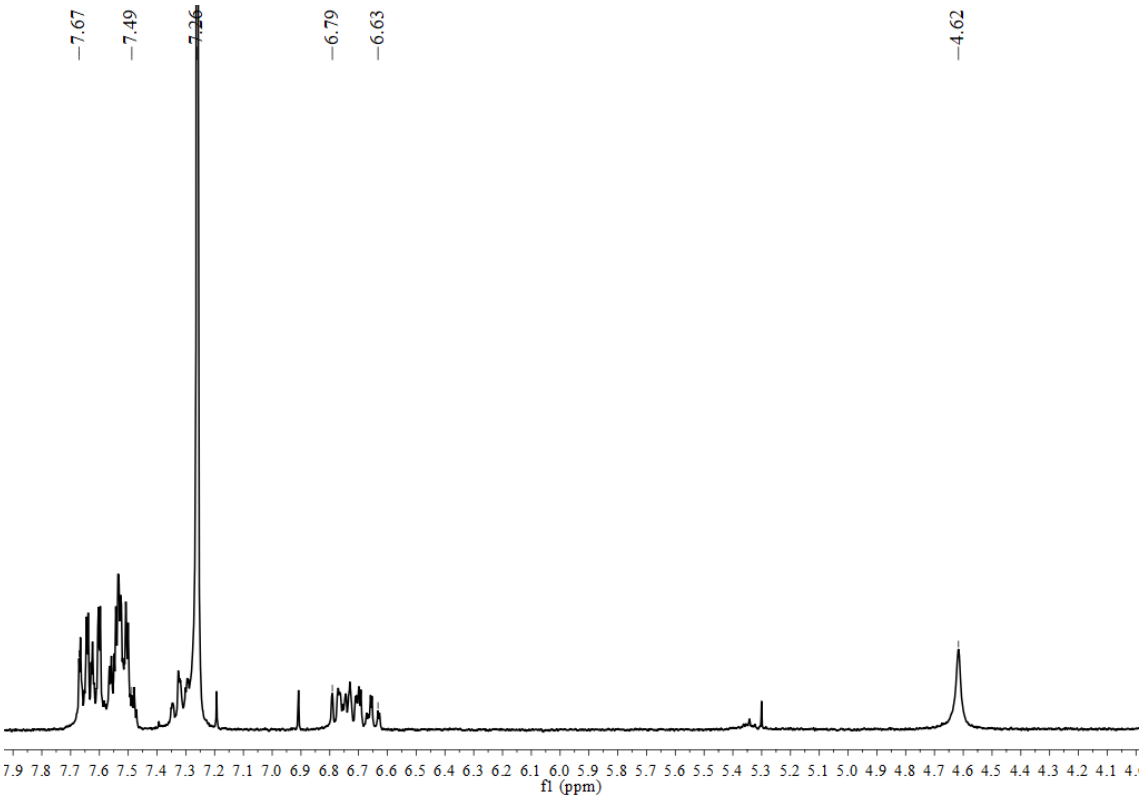

Figure S11. ^{1}H NMR spectrum of complex [Au(C_6Cl_5)(PNH_2)] (**3**) in $CDCl_3$ 300

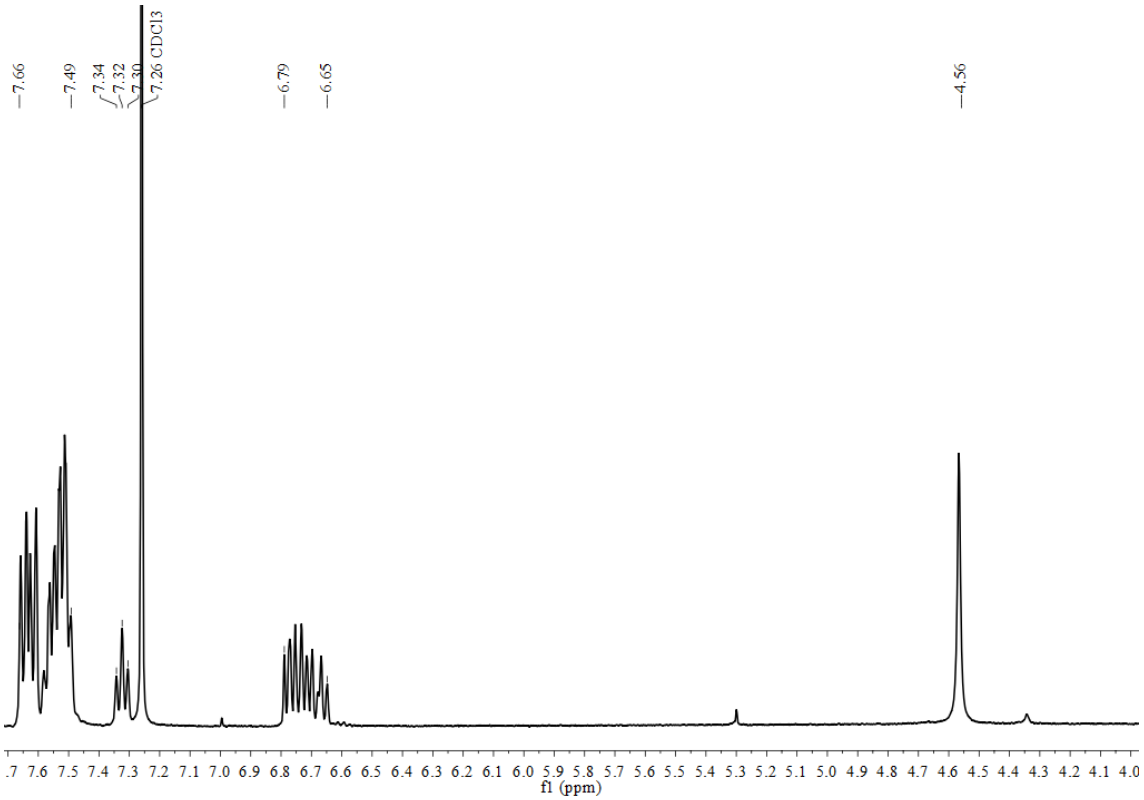

Figure S12. ^{1}H NMR spectrum of complex [Au(*o*-C_6BrF_4)(PNH_2)] (**4**) in $CDCl_3$ 400

4. ^{19}F NMR spectra (282 MHZ, 298K)

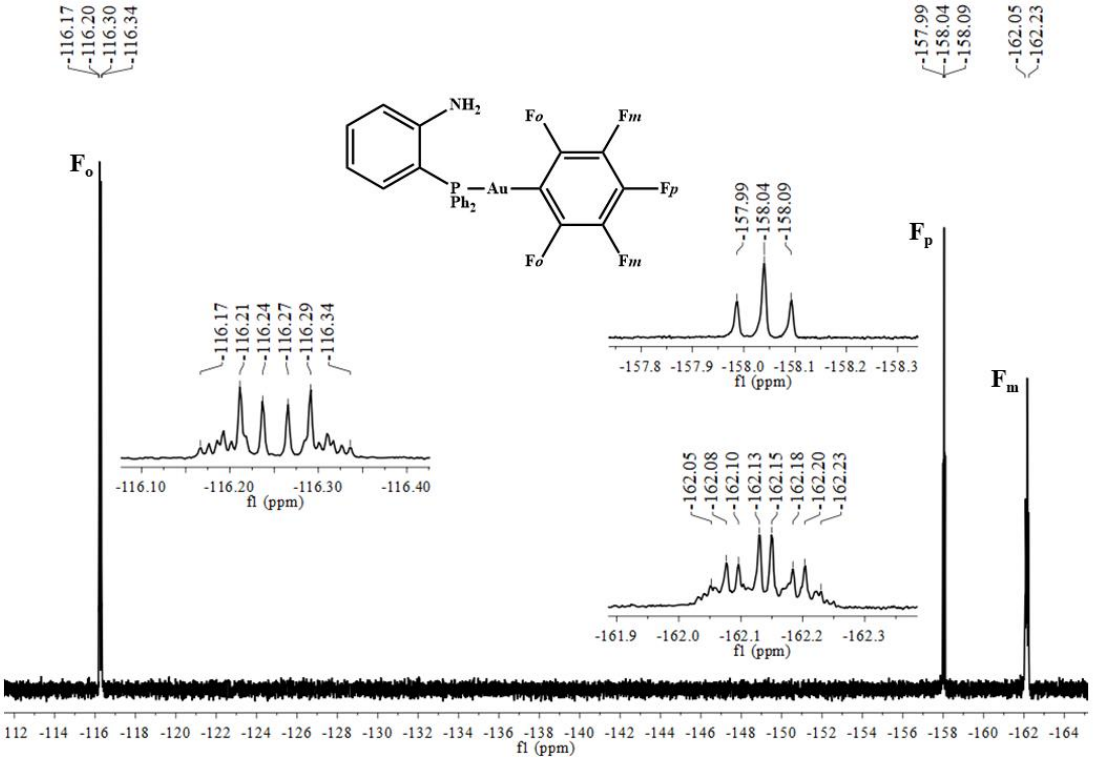

Figure S13. ^{19}F NMR spectrum of complex Au(C_6F_5)(PNH_2)] (**1**) in $CDCl_3$ 400

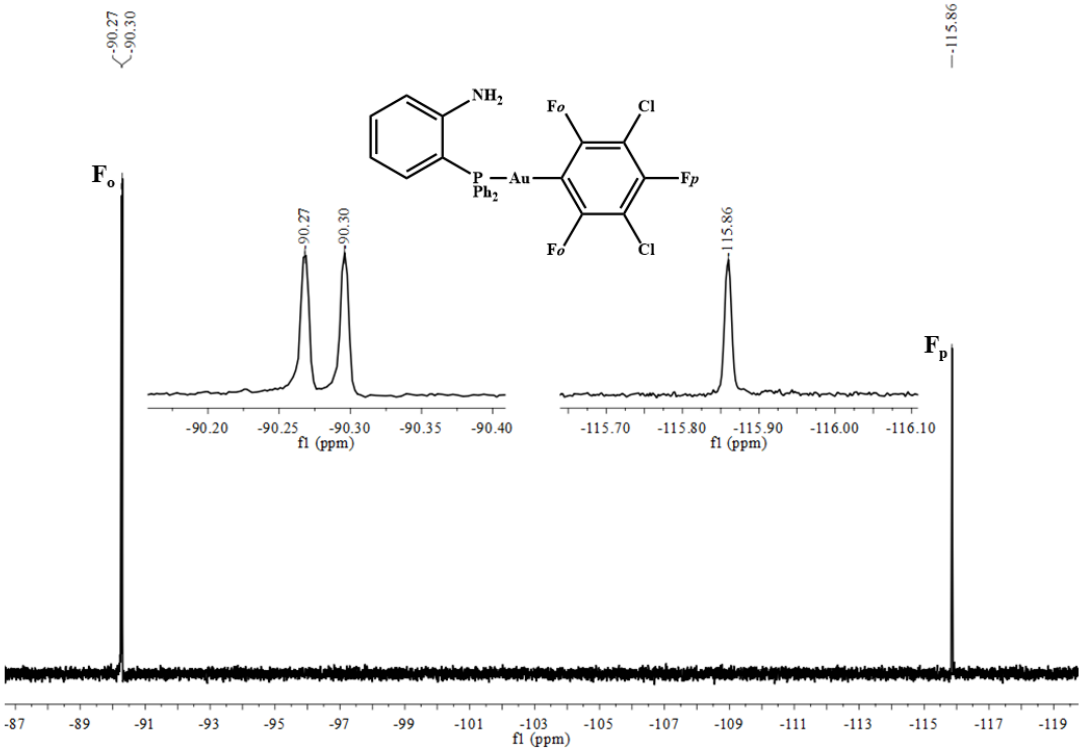

Figure S14. ^{19}F NMR spectrum of complex [Au($C_6Cl_2F_3$)(PNH_2)] (**2**) in $CDCl_3$ 300

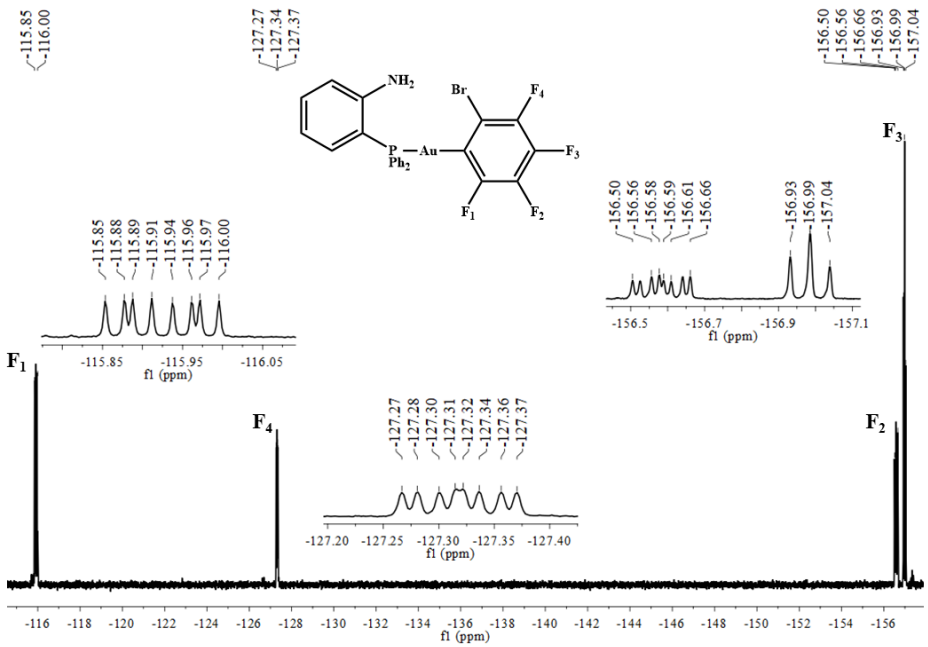

Figure S15. ^{19}F NMR spectrum of complex [Au(*o*-C_6BrF_4)(PNH_2)] (**4**) in $CDCl_3$ 400

5. $^{31}P\{1H\}$ NMR spectra (MHZ, 298K)

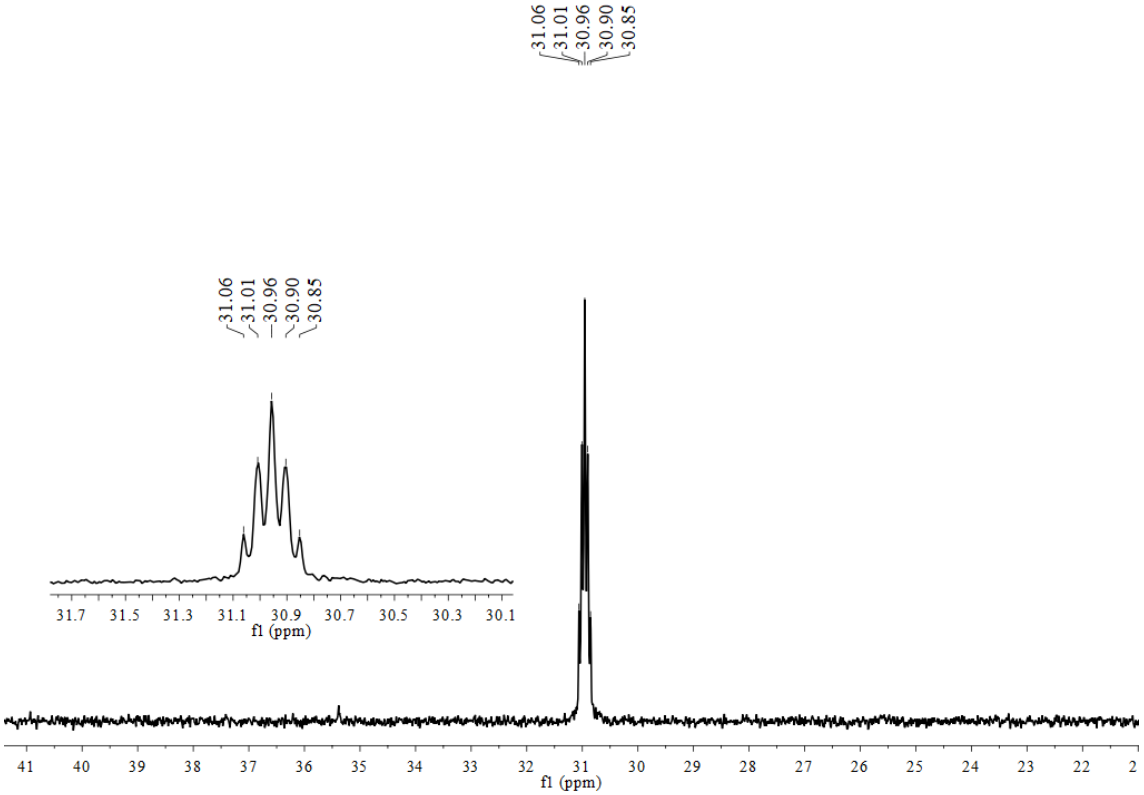

Figure S16. $^{31}P\{^1H\}$ NMR spectrum of complex [Au(C_6F_5)(PNH_2)] (**1**) in $CDCl_3$ 400

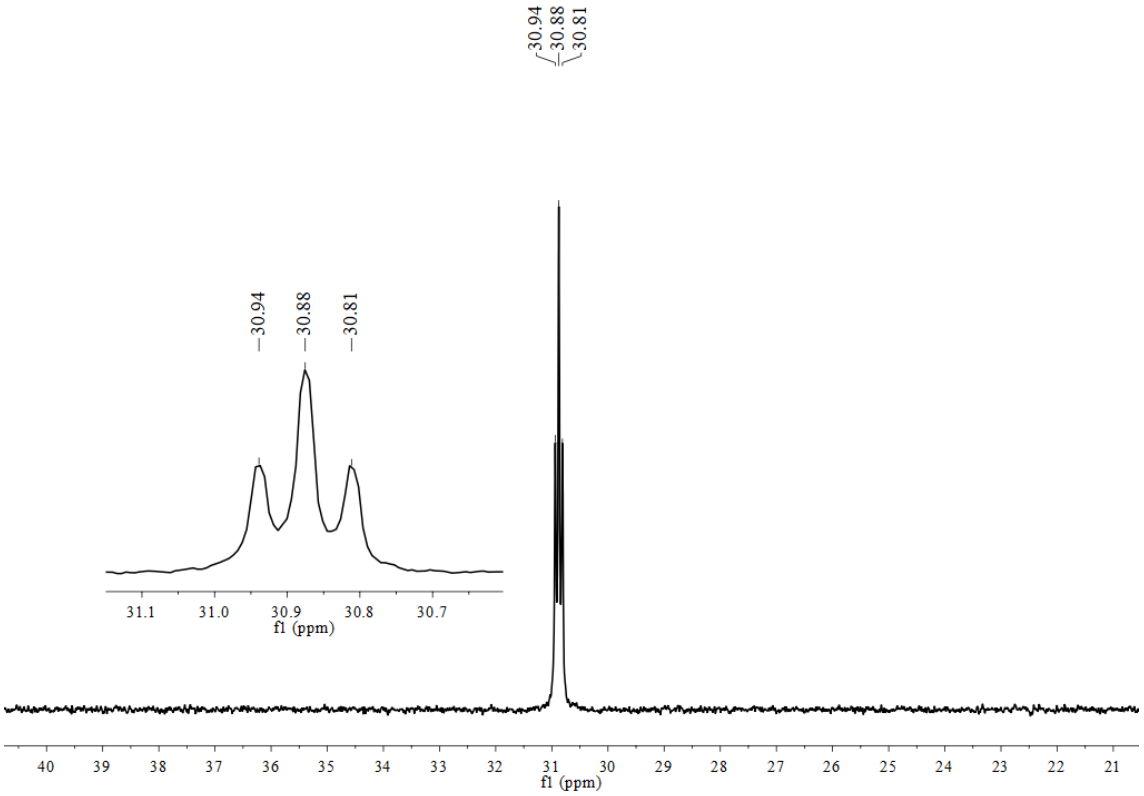

Figure S17. $^{31}P\{^{1}H\}$ NMR spectrum of complex $[Au(C_6Cl_2F_3)(PNH_2)]$ (**2**) in $CDCl_3$ 300

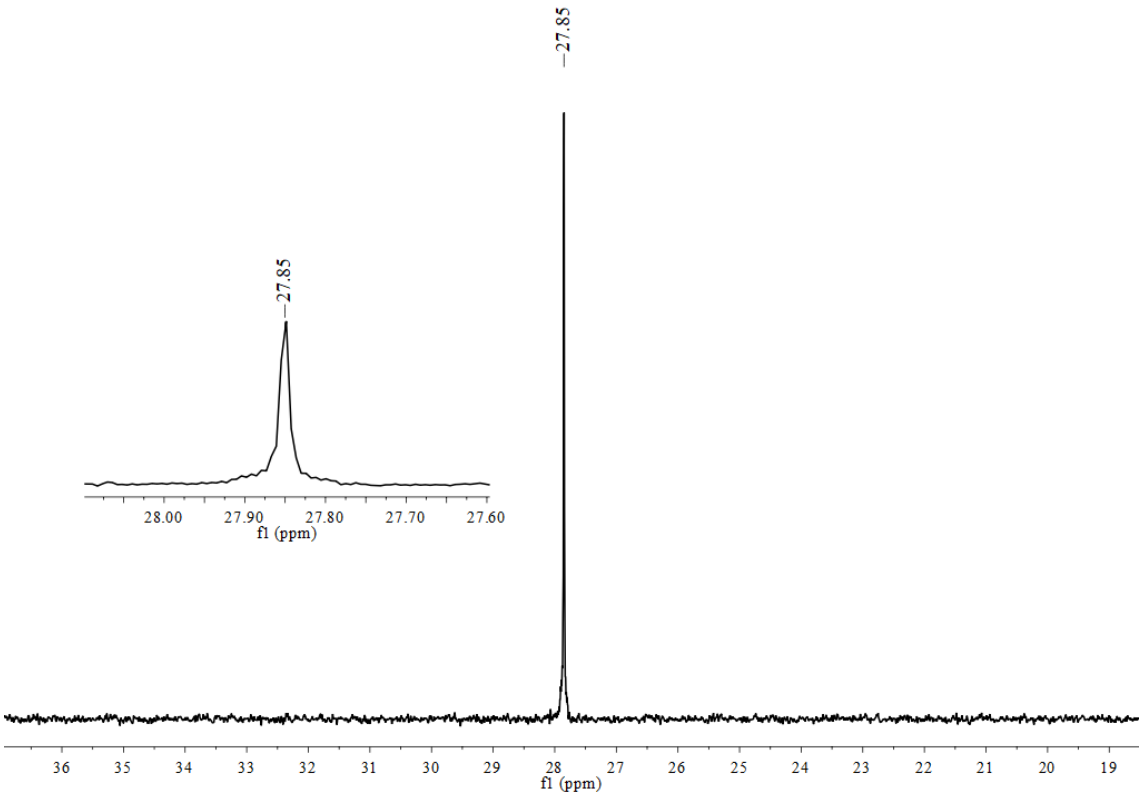

Figure S18. $^{31}P\{^{1}H\}$ NMR spectrum of complex $[Au(C_6Cl_5)(PNH_2)]$ (**3**) in $CDCl_3$ 300

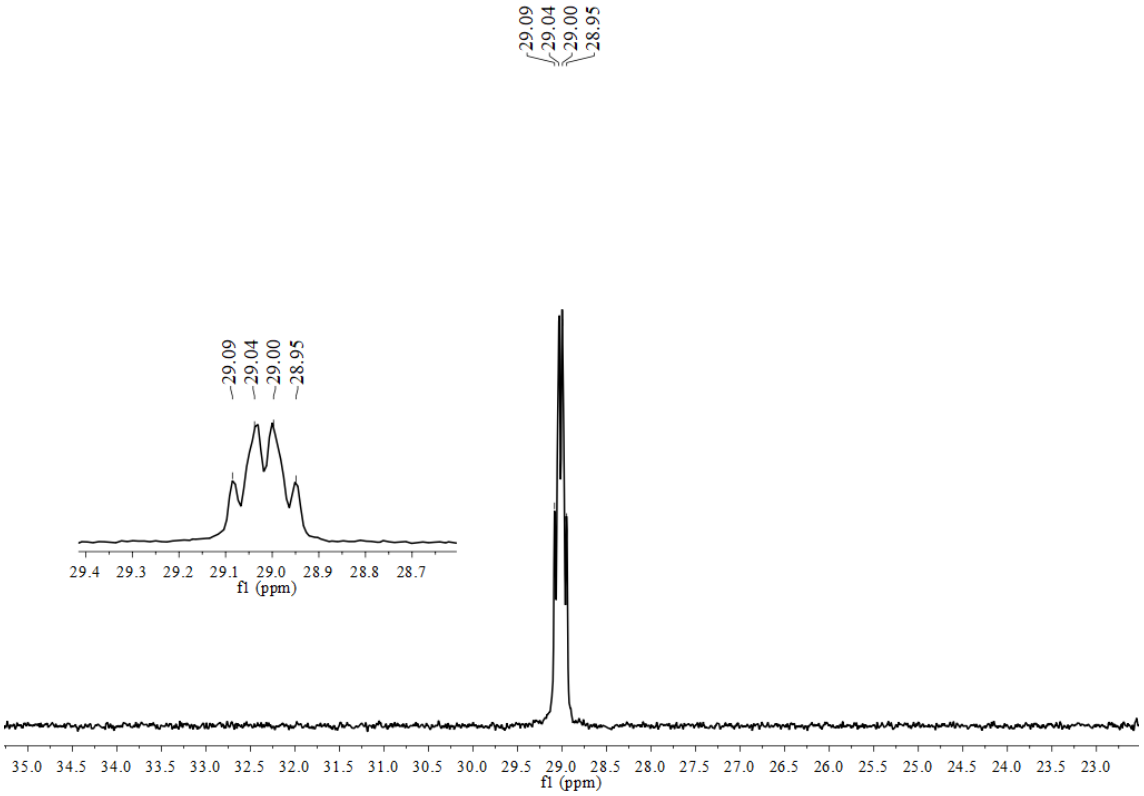

Figure S19. $^{31}P\{^{1}H\}$ NMR spectrum of complex [Au(*o*-C_6BrF_4)(PNH_2)] (**4**) in $CDCl_3$ 400

6. Single crystals X-ray diffraction analyses

Table S1. Data collection and structure refinement details for **1**, **2**, **3** and **4**.

	1	**2**	**3**	**4**
Chemical Formula	$C_{24}H_{16}AuF_5NP$	$C_{24}H_{16}AuCl_2F_3NP$	$C_{24}H_{16}AuCl_5NP$	$C_{24}H_{16}AuBrF_4NP$
Crystal habit	colorless	colorless	colorless	colorless
Crystal size/mm	0.060 × 0.026 × 0.014	0.143 × 0.121 × 0.049	0.162 × 0.059 × 0.020	0.283 × 0.096 × 0.084
Crystal system	Monoclinic	Monoclinic	Triclinic	Monoclinic
Space group	$P2_1/c$	$P2_1/n$	P-1	$P2_1/n$
a/Å	7.9453(7)	8.2765(5)	10.1789(11)	8.1842(11)
b/Å	12.0802(10)	11.9307(7)	10.6136(12)	12.0374(15)
c/Å	22.847(2)	22.5683(15)	11.2905(12)	23.570(3)
α/°	90	90	101.120(4)	90
β/°	98.012(3)	100.476(2)	93.797(4)	99.558(5)
γ/°	90	90	93.764(4)	90
V/Å^3	2171.5(3)	2191.3(2)	1190.4(2)	2289.8(5)
Z	4	4	2	4
Dc/g cm^{-3}	1.962	2.044	2.019	2.037
M	641.31	674.21	723.56	702.22
F(000)	1224.0	1288.0	692.0	1328.0
T/K	118(2)	100(2)	100(2)	300(2)
2θmax/°	55.930	55.788	55.82	51.362
μ(Mo-Kα)/mm^{-1}	6.903	7.069	6.822	8.284
No. refl. Measured	41168	60441	29401	111607
No. unique refl.	5200	5214	5660	4329
Rint	0.0679	0.0357	0.0313	0.0437
R[F>2σ(F)][a]	0.0678	0.0352	0.0278	0.0726
wR[F2, all refl.][b]	0.1443	0.0865	0.0620	0.1549
No. of refl. Used [F>2σ(F)]	5200	5214	5660	4329
No. of parameters	286	289	298	286
No. of restrains	0	0	0	0
S [c]	1.216	1.156	1.172	1.342
Max. residual electron density/e·Å^{-3}	1.30	1.67	1.39	2.223

[a] R: $(F) = \sum||F_o| - |F_c||/\sum|F_o|$.

[b] wR: $(F^2) = [\sum\{w(F_o^2-F_c^2)^2\}/\sum\{w(F_o^2)^2\}]^{0.5}$; $w^{-1} = \sigma^2(F_o^2) + (aP)^2 + bP$, where $P = [F_o^2 + 2F_c^2]/3$ and a and b are constants adjusted by the program.

[c] $S = [\sum\{w(F_o^2-F_c^2)^2\}/(n-p)]^{0.5}$, where n is the number of data and p the number of parameters.

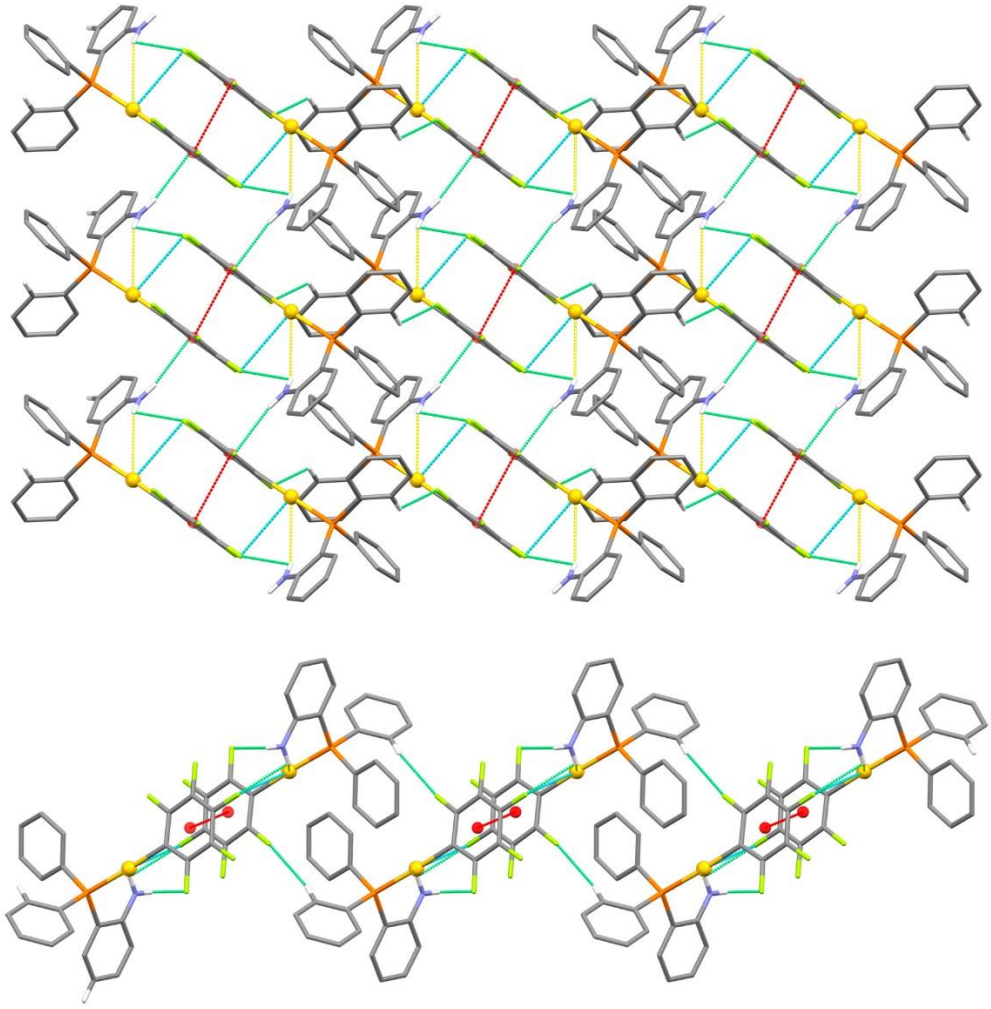

Figure S20. Two different views of the supramolecular arrangement in the crystal structure of **1**, depicting the intramolecular N-H··Au hydrogen bonds (in yellow), the Au···F (in blue) and π-π stacking interactions between C_6F_5 rings (in red) within the dimers, and intermolecular N-H···F and C-H···F hydrogen bonds (in green) that give rise to the 3D network. Hydrogen atoms not involved in weak contacts have been omitted for clarity. Color code: yellow: gold; orange: phosphorus; blue: nitrogen; grey: carbon; white: hydrogen; light green: fluorine.

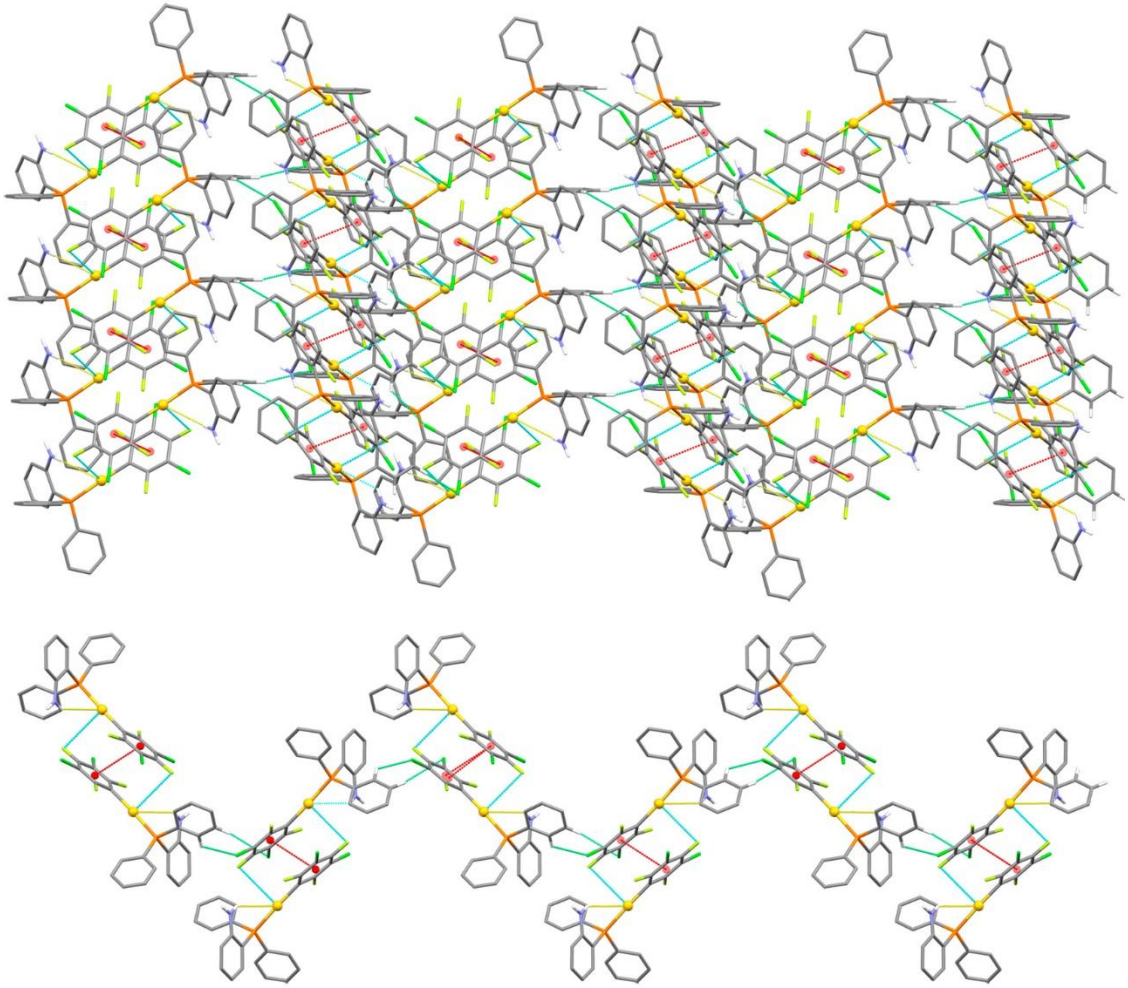

Figure S21. Two different views of the supramolecular arrangement in the crystal structure of **2**, depicting the intramolecular N-H··Au hydrogen bonds (in yellow), the Au···F (in blue) and π-π stacking interactions between $C_6Cl_2F_3$ rings (in red) within the dimers, and intermolecular C-H···Cl and C-H···F hydrogen bonds (in green) that give rise to the 3D network. Hydrogen atoms not involved in weak contacts have been omitted for clarity. Color code: yellow: gold; orange: phosphorus; blue: nitrogen; grey: carbon; white: hydrogen; green: chlorine; light green: fluorine.

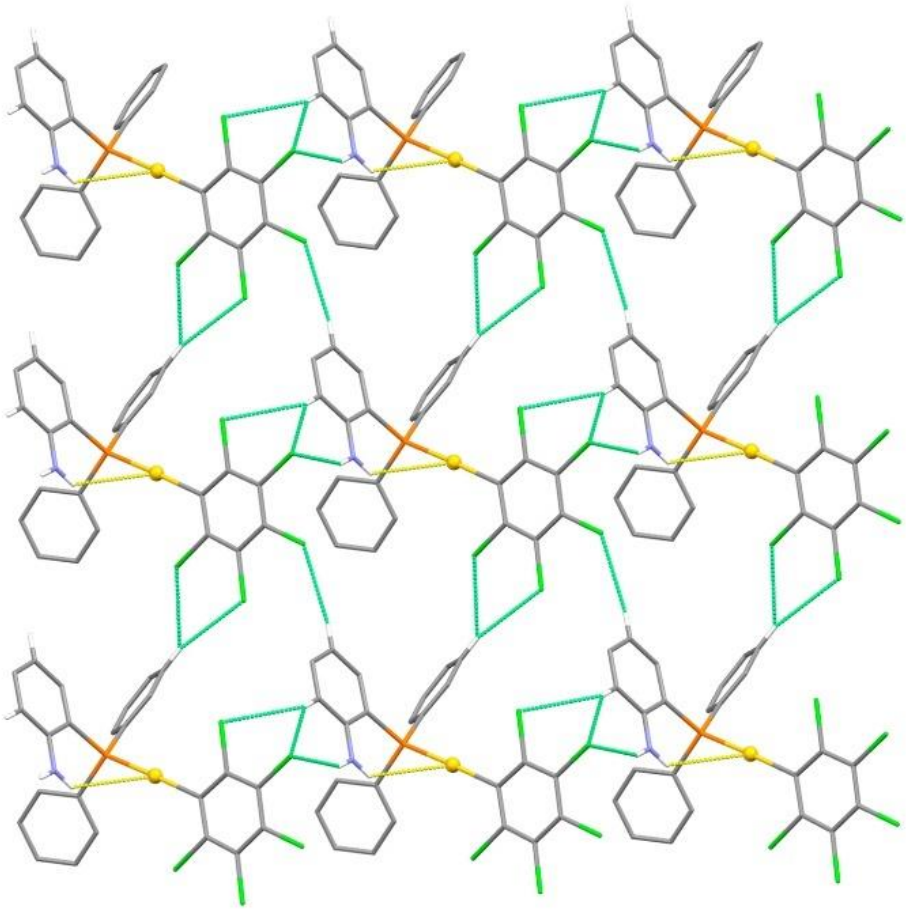

Figure S22. Supramolecular arrangement in the crystal structure of **3** viewed from the crystallographic *y* axis, depicting the N-H···Cl and C-H···Cl hydrogen bonds (in green) that give rise to the 2D network, and the intramolecular N-H···Au hydrogen bonds (in yellow). Hydrogen atoms not involved in weak contacts have been omitted for clarity. Color code: yellow: gold; orange: phosphorus; blue: nitrogen; grey: carbon; white: hydrogen; green: chlorine.

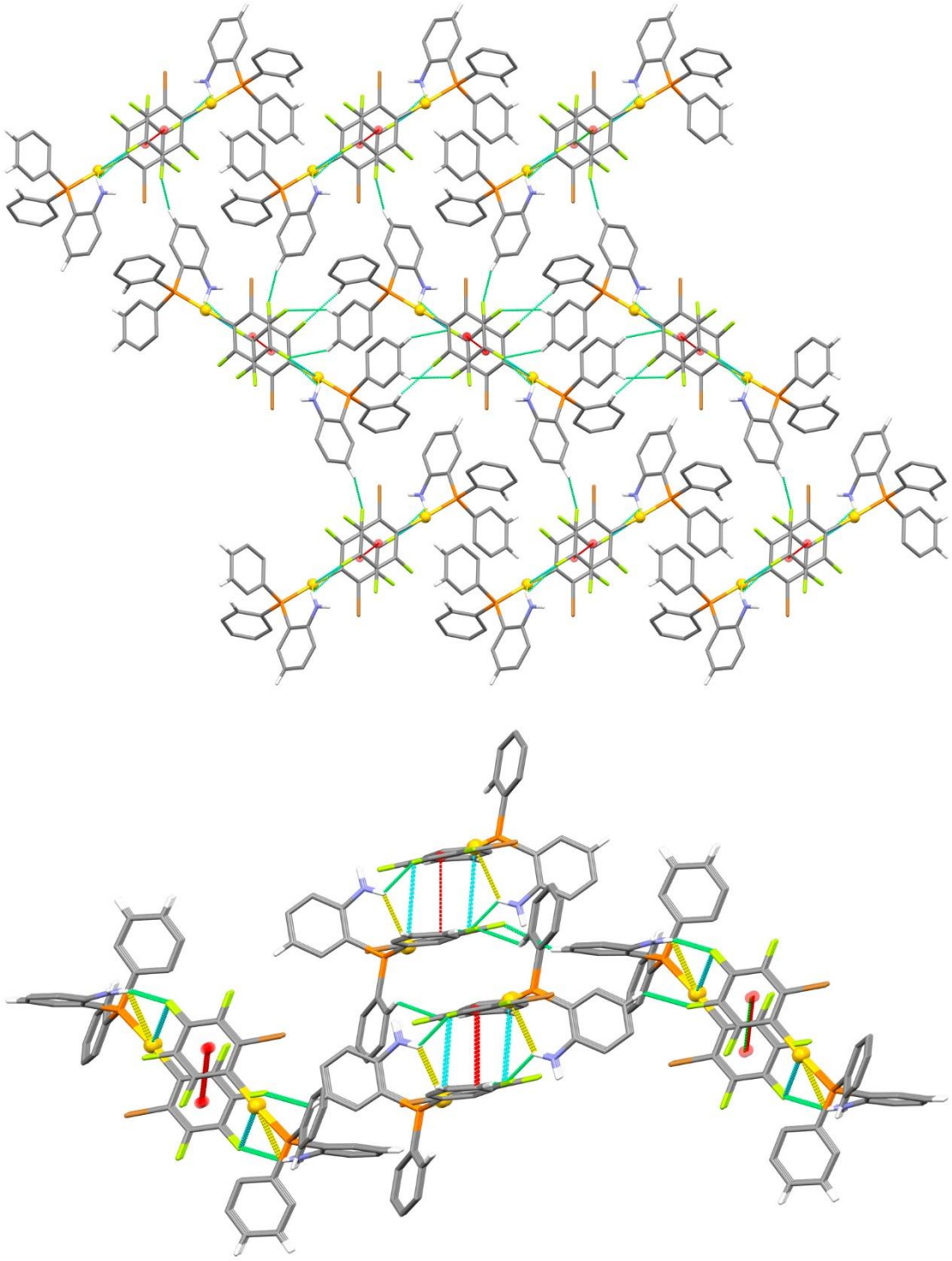

Figure S23. Two different views of the supramolecular arrangement in the crystal structure of **4**, depicting the C-H···F hydrogen bonds (in green) that give rise to the 3D network depicting the intramolecular N-H··Au hydrogen bonds (in yellow), the Au···F (in blue) and π-π stacking interactions between C_6BrF_4 rings (in red) within the dimers, and intermolecular C-H···F hydrogen bonds (in green) that give rise to the 3D network. Hydrogen atoms not involved in weak contacts have been omitted for clarity. Color code: yellow: gold; orange: phosphorus; blue: nitrogen; grey: carbon; white: hydrogen; brown: bromine; light green: fluorine.

II. Computational Studies

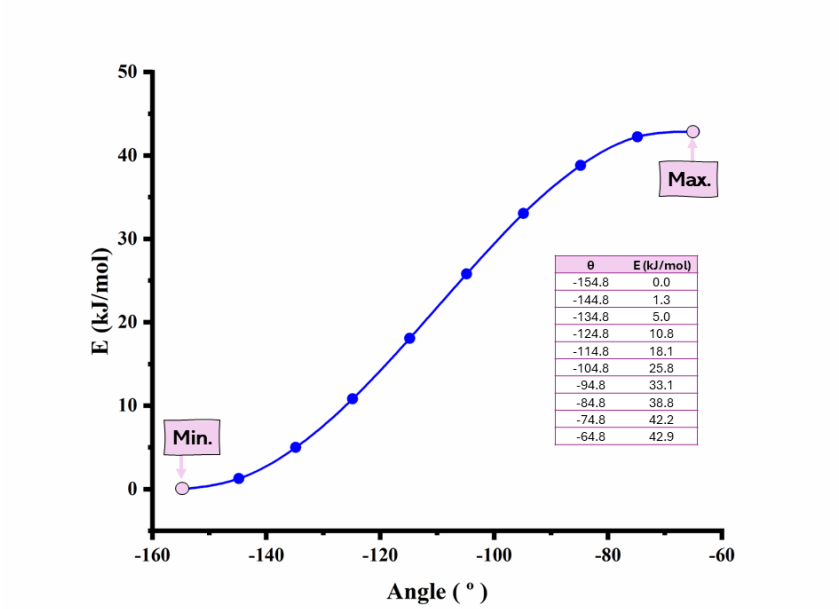

Figure S24. Potential energy profile for complex **1**. The plot depicts the variation in relative energy as a function of the H-N-C-C dihedral angle, calculated at 10° intervals.

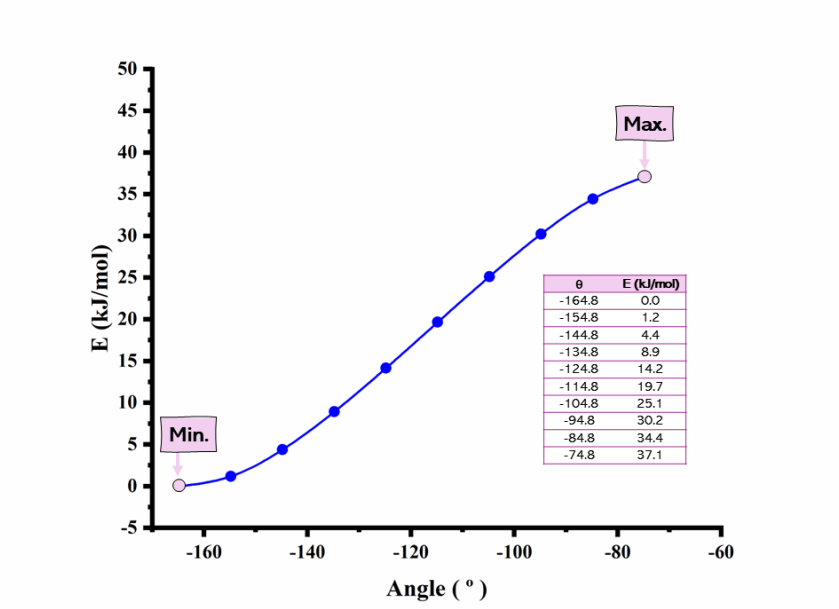

Figure S25. Potential energy profile for complex **2**. The plot depicts the variation in relative energy as a function of the H-N-C-C dihedral angle, calculated at 10° intervals.

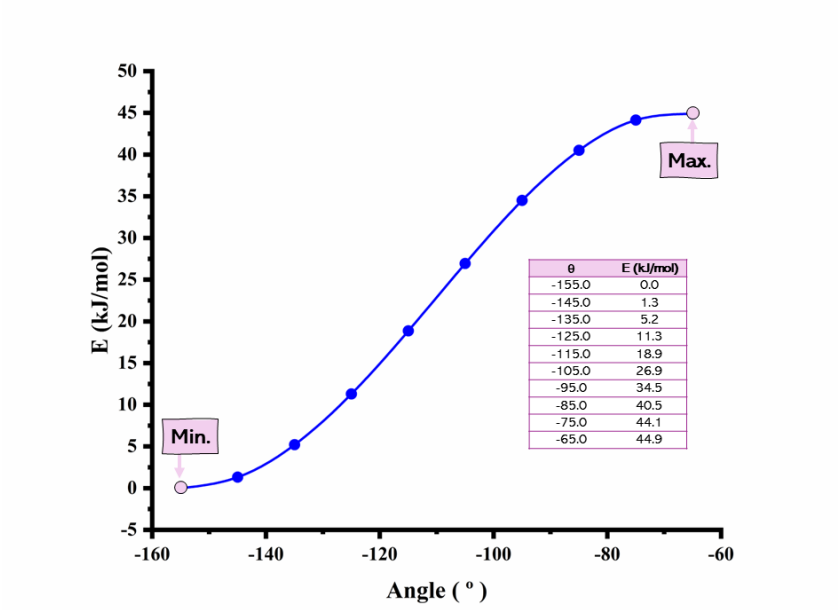

Figure S26. Potential energy profile for complex **3**. The plot depicts the variation in relative energy as a function of the H-N-C-C dihedral angle, calculated at 10° intervals.

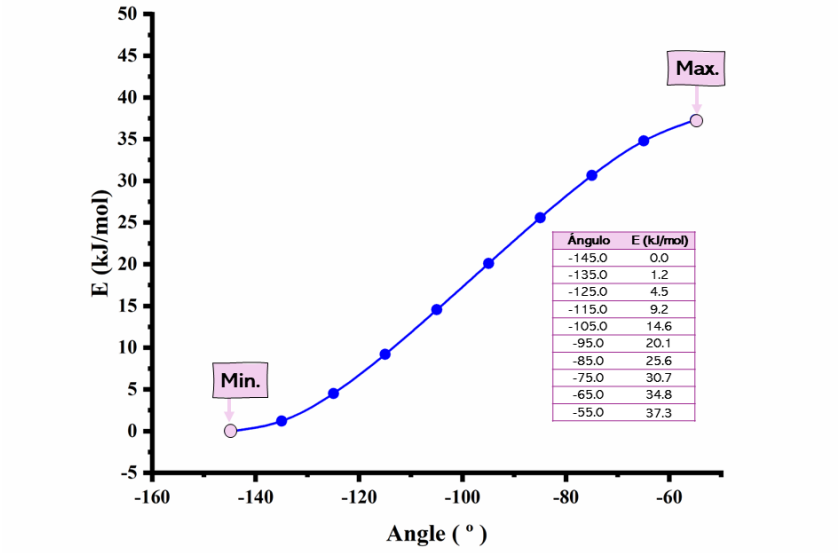

Figure S27. Potential energy profile for complex **4**. The plot depicts the variation in relative energy as a function of the H-N-C-C dihedral angle, calculated at 10° intervals.

Table S2. Tables of results obtained after conducting frequency calculations for the four molecules (**1**-**4**) and their three corresponding models labelled as **a**, **b**, and **c**.

	Sum of electronic and thermal Free Energies (kJ/mol)		
Comformer	**a**	**b**	**c**
Compound **1**	0	52.6	10.0
Compound **2**	0	48.3	9.6
Compound **3**	0	54.4	10.7
Compound **4**	0	47.7	14.6